Lowering sulfur density in margin to trigger Molybdenum disulfide nanoarray growth into branches for boosting their hydrogen evolution reaction

Ruifeng Qi[a], Xiaohua Qiao[a], Jinhong Hou[a],Tianyu Zhang[a], Junqi Liu[a], Qin Liu[a],Feng Gao[a]and QingsongHuang[a,b]*

[a] School of Chemical Engineering, Sichuan University, Chengdu 610065, China.

[b] Tianfu Jiangxi Laboratory, Chengdu 610065,China

1. The MoS_2 nanoarrays grown at different S/MoO_3 molar ratios.

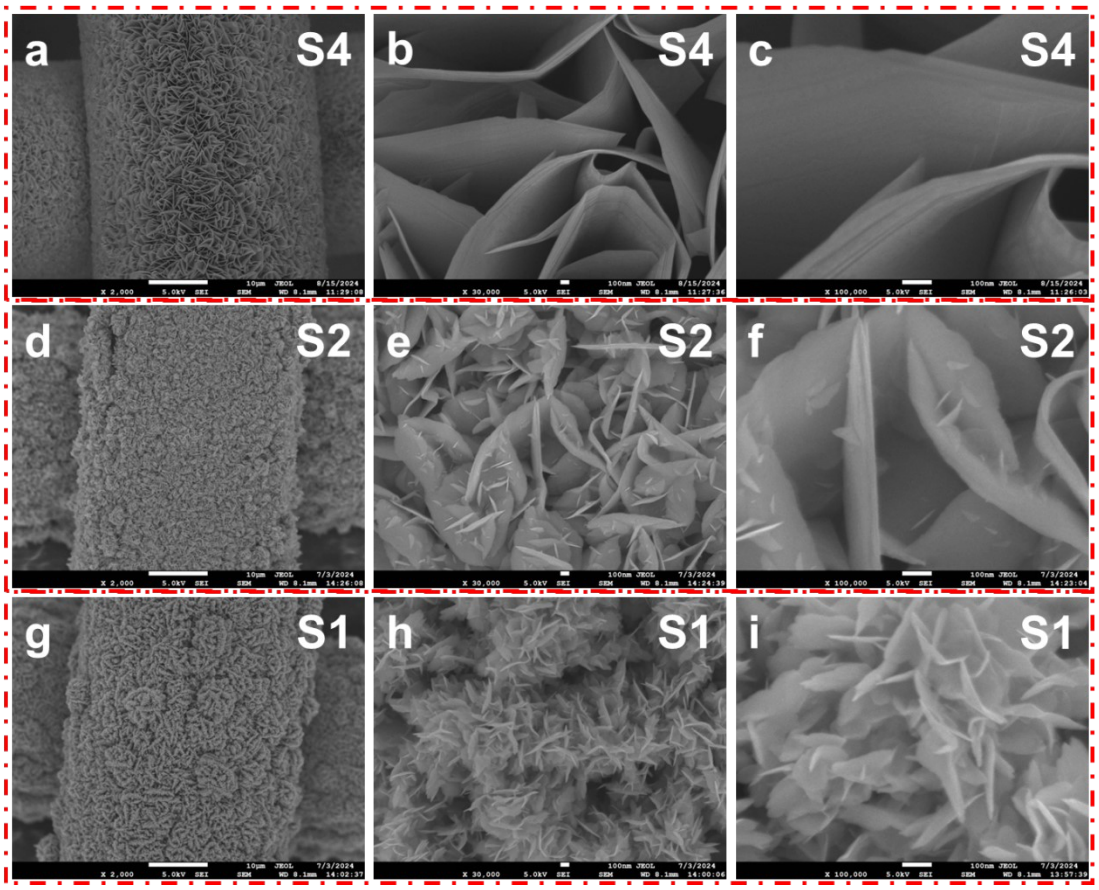

Fig. S1 (a-c) Morphology of sample S4 at different magnifications. (d-f)

Morphology of sample S2 at different magnifications. (g-i) Morphology of sample S1 at different magnifications.

2. The MoS_2 nanoarrays grown and etched with different S/MoO_3 molar ratios.

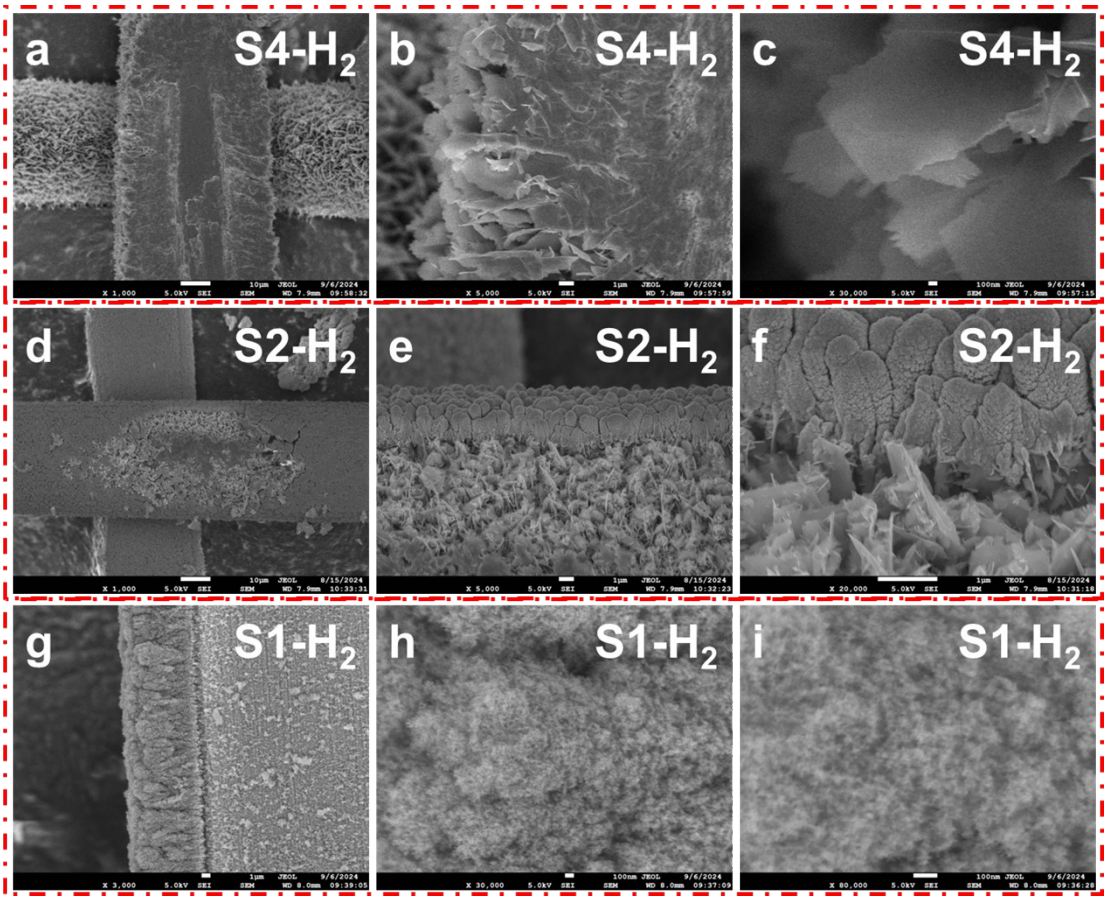

Fig. S2 (a-c) Morphology of sample S4-H_2 at different magnifications. (d-f) Morphology of sample S2-H_2 at different magnifications. (g-i) Morphology of sample S1-H_2 at different magnifications.

3. Sulfur vacancies at the edge of MoS_2 nanosheets

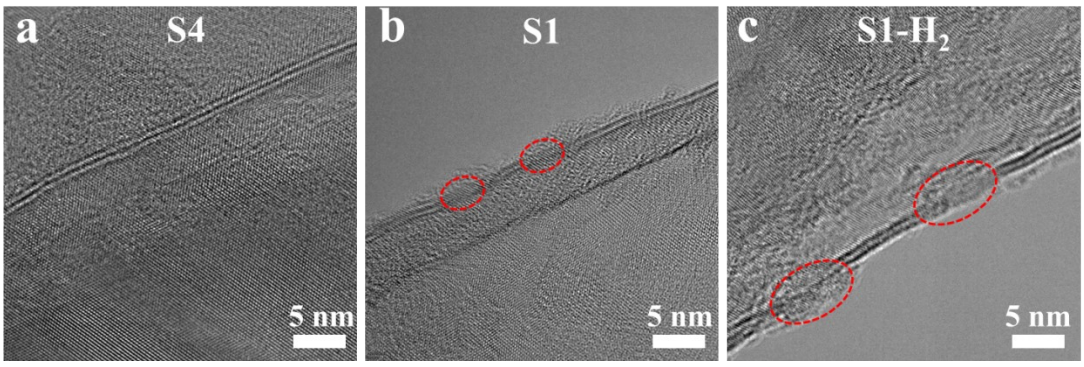

Fig. S3(a) HRTEM image of S4 showing the MoS_2 crystal structure of 2 ML. (b)

HRTEM image of S1 showing MoS_2 edge defects. (b) HRTEM image of S1-H_2 showing more MoS_2 edge defects than S1.

4. The XPS spectrum of S4, S1 and S1-H_2.

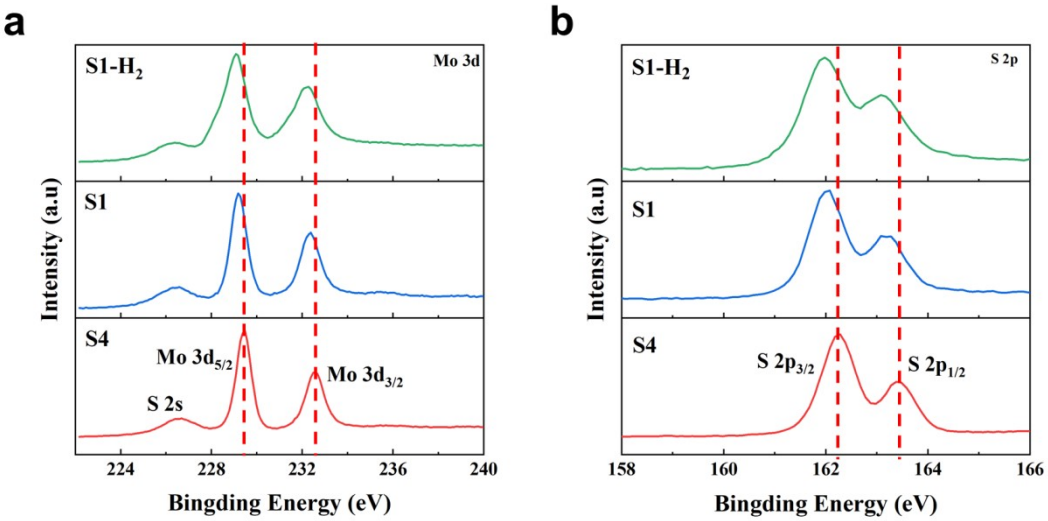

Fig. S4 XPS images of S4, S1 and S1-H_2. The Mo 3d and S 2p peaks from S4, S1 to S1-H2 are shifted to lower binding energies, indicating an increase in electron density around the Mo and S sites.

5. The ESR pattern of S4, S1 and S1-H_2.

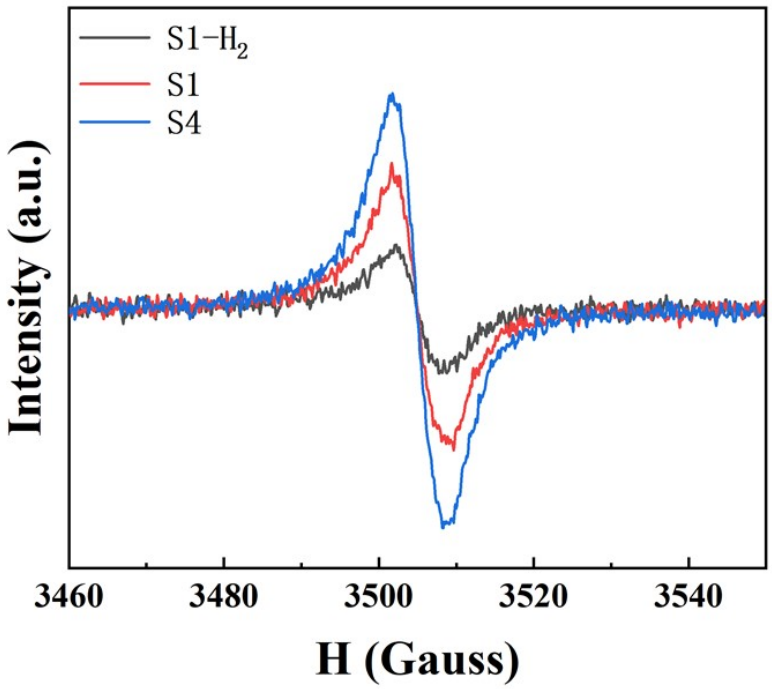

Fig. S5 Electron spins resonance spectra of various MoS_2 samples. The S signal is attributed to Mo-S bonding; higher intensity indicates lower S vacancy concentration.

6. The XRD pattern of Mo mesh, S4, S1 and S1-H_2.

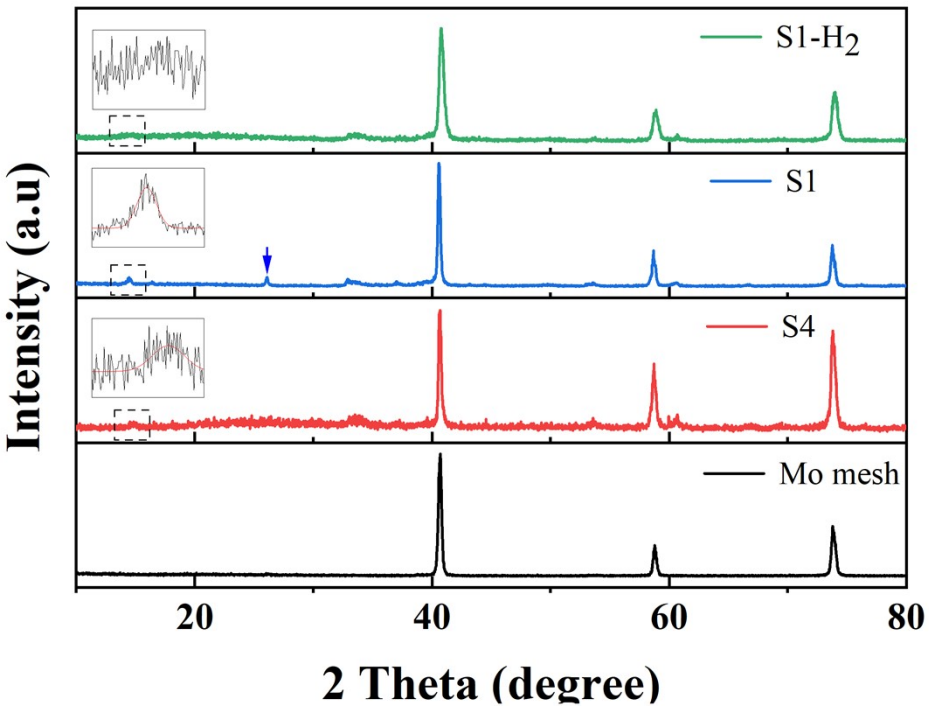

Fig. S6 XRD pattern of Mo mesh, S4, S1 and S1-H_2. The three most substantial peaks are from Mo. Most of the other characteristic peaks are from 2H-MoS_2 (standard PDF #87-2416), and only S1 is observed near 26° with a peak from the MoO_2 feature. The peaks from MoS_2 are weak, indicating that the MoS_2 structural domain is minimal.

7. The TEM image of S1-H_2.

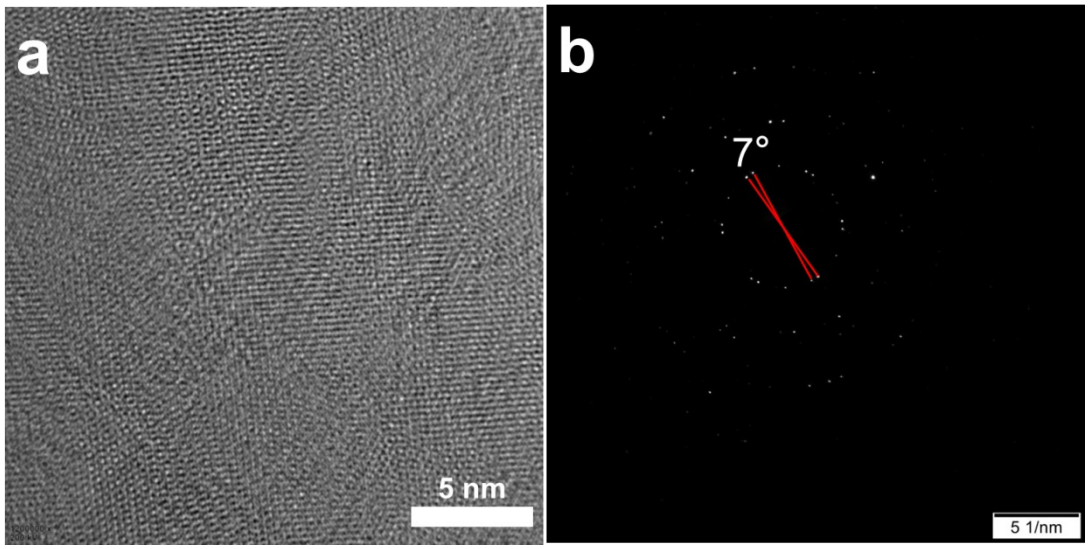

Fig. S7 (a) Moiré patterns can be observed in some parts of the HRTEM image of S1-H_2, suggesting the slight rotation between MoS_2 layers. (b) The angle of rotation between the MoS_2 was estimated by SAED to be approximately 7°.

Supplementary Table 1: Summary of the representative MoS_2 electrocatalysts for HER at higher current densities.

Catalyst	Media	η_{10} (mV vs RHE)	η_{100} (mV vs RHE)	Tafel slope (mV/decade)	Stability
This work	**0.5M H_2SO_4**	**182**	**238**	**63**	**24 h (η100)**
HDP-MoS_2[1]	0.5M H_2SO_4	385	500	109	10000 s (η10)
Oxygen-Incorporated MoS_2[2]	0.5M H_2SO_4	120	300 (η126.5)	55	3000 cycles
PRMoSX@CC[3]	0.5M H_2SO_4	-	300 (η80)	49	3000 cycles
$MoS_2/NiPS_3$-1[4]	1.0M KOH	112	235	64	100 h (η10)
MoS_2@rGo/Mo[5]	1M H_2SO_4	172	292	52	12 h (η10)
Co_3S_4-MoS_2[6]	1.0M KOH	-	260	68.3	100 h (η100)
FeS/1T-MP MoS_2@rGO[7]	1.0M KOH	102	256	104	1000 cycles
1T0.72-MoS_2@NiS_2[8]	0.5M H_2SO_4	138	302	42	16 h (η45)
Co_3O_4/MoS_2[9]	1.0 M KOH	205	230 (η60)	128	14 h (η10)
MoO_2@E-MoS_2[10]	0.5M H_2SO_4	93	～240	154	70 h (η30)
MoO_2@E-MoS_2[10]	1.0 M KOH	99	～210	109	130 h (η15)
Ni-1T-MoS_2[11]	1.0 M KOH	199	250 (η50)	52.7	30 h (η12)
Pd-MoS_2[12]	1.0 M KOH	224.6	＞350	113	16 h (η10)
W-MoS_2@$FeNi_2S_4$/NF[13]	1.0 M KOH	130	～225	75.4	15 h (η10)
MoS_2-MoO_2/CW[14]	0.5M H_2SO_4	106	194	75.6	100 h (η10)
Co-MoS_2[15]	1.0 M KOH	67	330	67	24 h (η10)
$MoS_2/Ni(OH)_2$[16]	1.0 M KOH	185	252	73	1000 cycles
MCM@MoS_2-Ni[17]	0.5M H_2SO_4	161	275	81	24 h (η60)

$MoO_2/MoS_2/C$[18]	1.0 M KOH	91	269	49	20 h (η10)
$MoO_2/MoS_2/C$[18]	0.5M H_2SO_4	77	~240	41	20 h (η10)
WS_2-ox6[19]	0.5M H_2SO_4	-	152	54	-
NiS/MoS_2@FCP[20]	1.0 M KOH	128	283	70	10 h (η10)
CSC-MoS_2@CoS_2-24[21]	1.0 M KOH	241	433.2	169.8	20 h (η100)
Ni-Co-S@$NiMoO_4 \cdot xH_2O$/NF[22]	1.0 M KOH	90	-	77	50 h (η10)
WS_2/WN@CM[23]	1.0 M KOH	95	295.2		100 h (η200)
CoS/Ni_3S_2/NF[24]	1.0 M KOH	150	~260	104.9	24 h (η10)
Cr-NiS/NF[25]	1.0 M KOH	220	245 (η50)	60.79	100 h (η10)
BF–CoS[26]	1.0 M KOH	-	237(η50)	108	50 h (η50)
WS_2@WSe_2[27]	1.0 M KOH	52	154(η50)	58.7	52 h (η10)
V-NiS/CF[28]	1.0 M KOH	196	357	87	36 h (η100)

8. CV curves of S4,S2,S1,S4-H_2,S2-H_2 and S1-H_2.

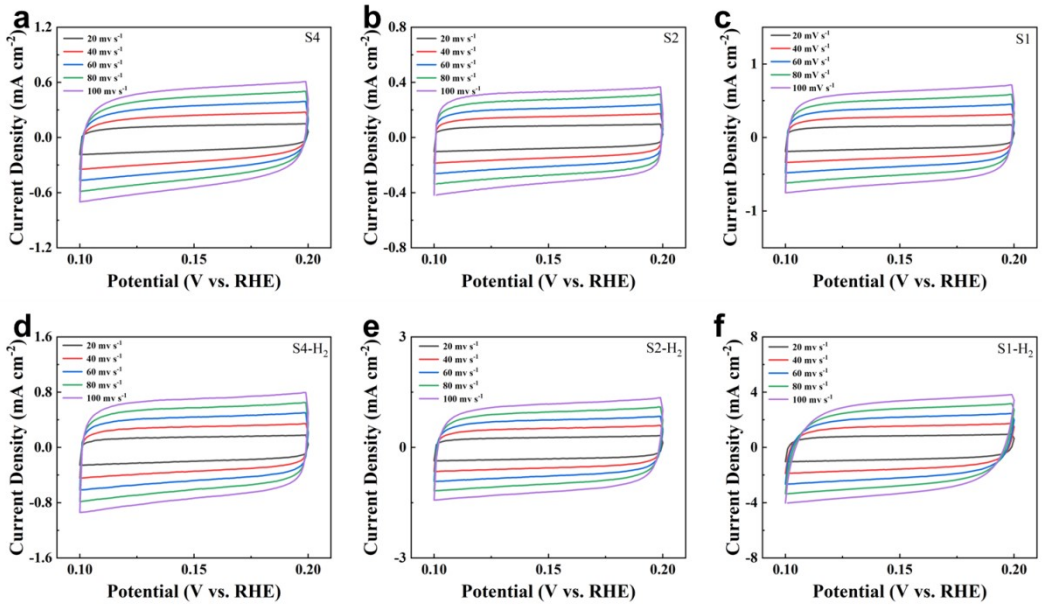

Fig. S8 CV curves of S4,S2,S1,S4-H_2,S2-H_2 and S1-H_2 in the region of 0.1-0.2 V (vs. RHE).

9. XRD analyses after the 24-hour constant-current test

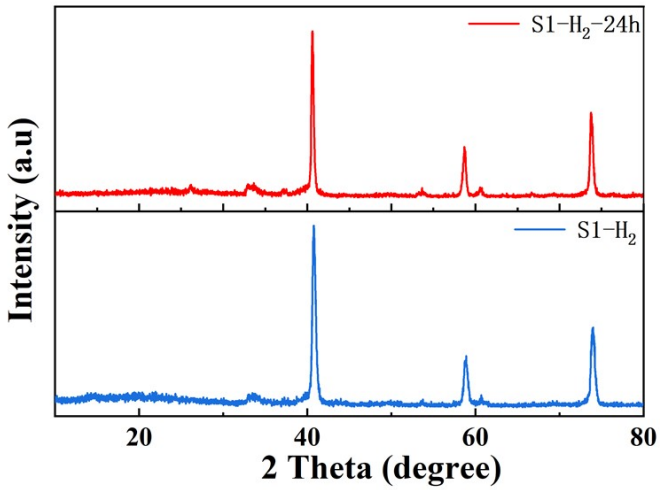

Fig. S9 XRD image of S1-H_2 after 24 h CP test. A comparison with the original sample revealed no significant changes in the XRD patterns.

10. SEM analyses after the 24-hour constant-current test

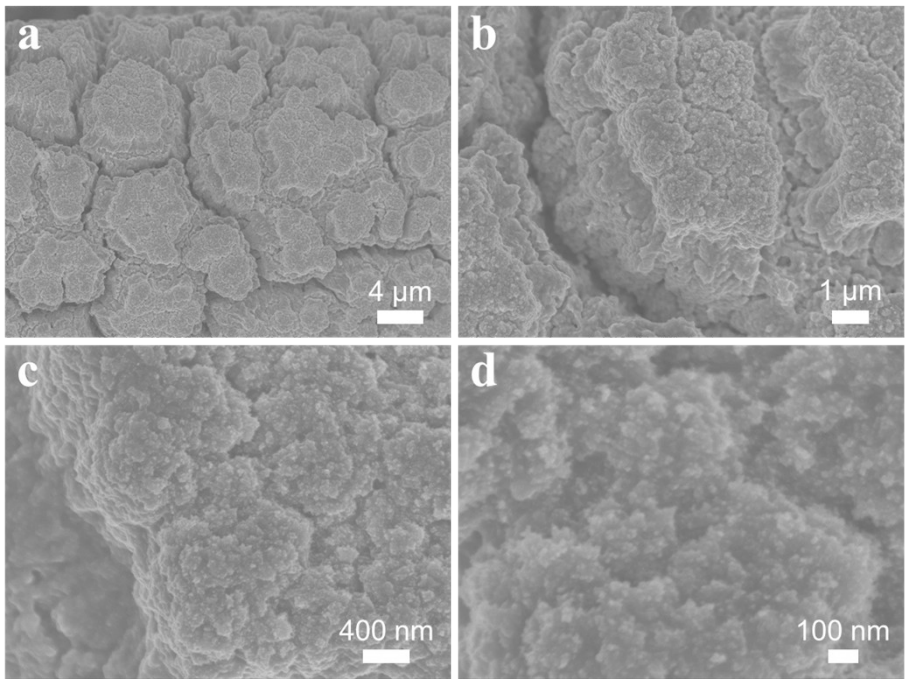

Fig. S10 SEM image of S1-H2 after 24 h CP test, MoS2 nano-arrays show micro-cracks

11. Growth of MoS_2 nanoarrays.

The name of the equipment is called high-frequency induction heating furnace. Fig. S11 shows a sketch of the entire device. Fig. S11(b) shows a cross-sectional view of the corundum crucible. Copper coil damage caused by high temperatures is prevented by passing cooling water through the coil. When the power is turned on and current is applied to the coil, high frequency dynamic magnetic field will be generated in the coil.

The dynamic magnetic field is coming from the field changing with time. Otherwise, we call it as static field. If we use "B" as the intensity of the magnetic field, the "B" changing with the time can be expressed as the function: $B=\frac{\mu_0 * N * I}{L}$, where the μ_0 is permeability of vacuum, and N represents turns per

coil, and L is loop length，and I is electric current. The induction furnace equipment utilises an IGBT power supply. The function of this power supply is to rectify the negative signal of the current to the positive signal, thus maintaining the direction of the magnetic field. Consequently, the direction of the force remains unaltered throughout the experiment. So I=$I_m * |\sin(\omega t + \varphi)|$. Where the amplitude of the alternating current is represented by I_m, the angular frequency by ω, and the initial phase by φ. Since the ω= 2πf , f is frequency，therefore the B= $\frac{\mu_0 * N}{L} * I_m * |\sin(2\pi f t + \varphi)|$. Here, a current frequency of 50 kHz was adopted.

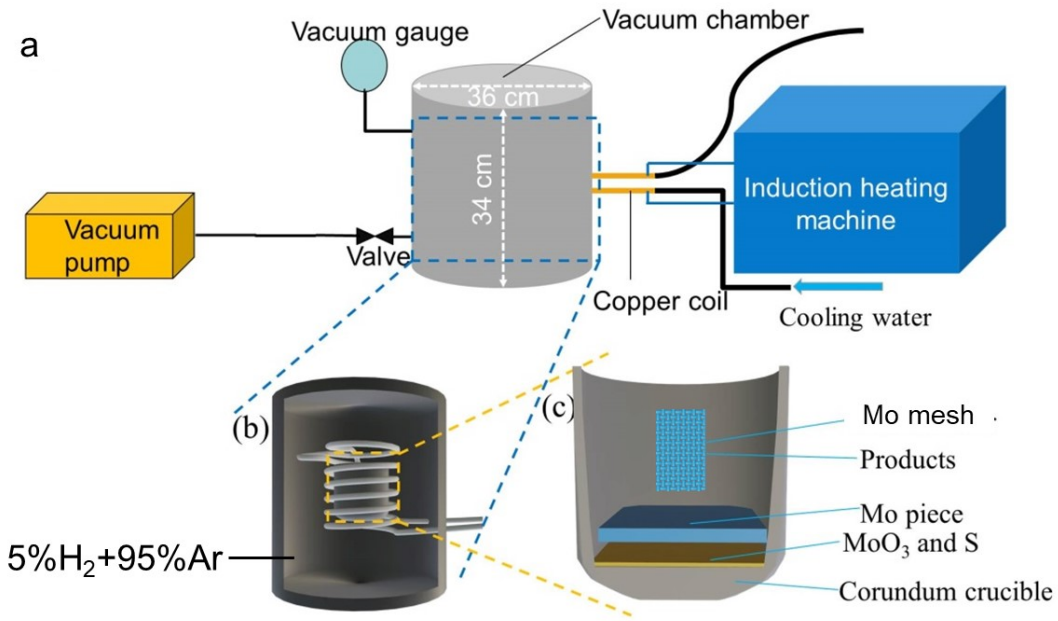

Fig. S11 Sketch of high-frequency induction-heated furnaces.

References:

1. S. Su, Q. Zhou, Z. Zeng, D. Hu, X. Wang, M. Jin, X. Gao, R. Nötzel, G. Zhou, Z. Zhang and J. Liu, *ACS APPL MATER INTER*, 2018, **10**, 8026-8035.
2. J. Xie, J. Zhang, S. Li, F. Grote, X. Zhang, H. Zhang, R. Wang, Y. Lei, B. Pan and Y. Xie, *J AM*

CHEM SOC, 2013, **135**, 17881-17888.

3. X. Huang, M. Leng, W. Xiao, M. Li, J. Ding, T. L. Tan, W. S. V. Lee and J. Xue, *ADV FUNCT MATER*, 2017, **27**.

4. Y. Liu, Y. Chen, Y. Tian, T. Sakthivel, H. Liu, S. Guo, H. Zeng and Z. Dai, *ADV MATER*, 2022, **34**.

5. B. K. Barman, D. Das and K. K. Nanda, *J MATER CHEM A*, 2017, **5**, 18081-18087.

6. J. Luo, Y. Zhou, Y. Tuo, Y. Gu, X. Wang, Q. Guo, C. Chen, D. Wang, S. Wang and J. Zhang, *APPL MATER TODAY*, 2022, **26**, 101311.

7. Y. Hou, C. Zhou, S. Bai, S. Yang, F. Yang, B. Yang and X. Zeng, *INT J HYDROGEN ENERG*, 2024, **90**, 191-198.

8. M. Liu, J. Wang, W. Klysubun, G. Wang, S. Sattayaporn, F. Li, Y. Cai, F. Zhang, J. Yu and Y. Yang, *NAT COMMUN*, 2021, **12**.

9. A. Muthurasu, V. Maruthapandian and H. Y. Kim, *Applied Catalysis B: Environmental*, 2019, **248**, 202-210.

10. X. Yu, F. Yan, Y. Zhao, B. Geng, X. Ma, L. Wu, X. Zhang and Y. Chen, *Applied Catalysis B: Environmental*, 2024, **343**, 123534.

11. G. Wang, G. Zhang, X. Ke, X. Chen, X. Chen, Y. Wang, G. Huang, J. Dong, S. Chu and M. Sui, *SMALL*, 2022, **18**, 2107238.

12. A. M. Teli, S. M. Mane, R. K. Mishra, W. Jeon and J. C. Shin, *INORGANICS*, 2025, **13**, 21.

13. X. Chai, X. Meng, Z. Li and X. Du, *INT J HYDROGEN ENERG*, 2025, **101**, 1044-1053.

14. L. He, M. Hu, Y. Qian, S. Cao, Y. Lu, M. Qin and L. Li, *J ELECTROANAL CHEM*, 2025, **986**, 119099.

15. Z. Li, C. Li, J. Chen, X. Xing, Y. Wang, Y. Zhang, M. Yang and G. Zhang, *J ENERGY CHEM*, 2022, **70**, 18-26.

16. Z. Zhu, H. Yin, C. T. He, M. Al Mamun, P. Liu, L. Jiang, Y. Zhao, Y. Wang, H. G. Yang, Z. Tang, D. Wang, X. M. Chen and H. Zhao, *ADV MATER*, 2018, **30**, 1801171.

17. H. Zhang, L. Yu, T. Chen, W. Zhou and X. W. D. Lou, *ADV FUNCT MATER*, 2018, **28**, 1807086.

18. F. Gong, M. Liu, S. Ye, L. Gong, G. Zeng, L. Xu, X. Zhang, Y. Zhang, L. Zhou, S. Fang and J. Liu, *ADV FUNCT MATER*, 2021, **31**, 2101715.

19. L. Yang, X. Zhu, S. Xiong, X. Wu, Y. Shan and P. K. Chu, *ACS APPL MATER INTER*, 2016, **8**, 13966-13972.

20. Y. Zheng, P. Tang, X. Xu and X. Sang, *J SOLID STATE CHEM*, 2020, **292**, 121644.

21. Y. Cheng, X. Zhou, Q. Pan, L. Zhang, Y. Cao and T. Qian, *RARE METALS*, 2023, **42**, 3024-3033.

22. Z. Gao, T. Zhang, D. Xu, P. Liu, H. Liu, H. Li, Y. Liu, F. Yu and G. Wang, *J CATAL*, 2024, **434**, 115540.

23. J. Zhao, L. Li, H. Jiang, H. Tang, D. Chen, J. Yao, F. Du and G. Li, *APPL SURF SCI*, 2025, **680**, 161466.

24. H. Zhou and C. Xu, *APPL SURF SCI*, 2025, **705**, 163515.

25. J. Liu, C. Li, M. Chen, W. Xiao, S. Zhu, P. Lv and X. Yan, *APPL SURF SCI*, 2025, **709**, 163890.

26. M. S. Mohamed Saleem, P. Pazhamalai, N. U. H. Liyakath Ali, J. Chennakrishnan and S. J. Kim, *INT J HYDROGEN ENERG*, 2025, **156**, 150357.

27. X. Chi, X. Zhang, J. Zhao, Q. Wang, W. Yuan and X. Li, *INT J HYDROGEN ENERG*, 2025, **161**, 150735.

28. J. Sun, Z. Wei, Z. Zhang, Z. Wang, L. Xiao, Q. Liu, G. Hu and X. Liu, *INORG CHEM*, 2025, **64**, 11227-11235.